Ordered Binary Ionic Adlayers on a Au(110) Electrode: Coadsorption of Alkali Metal Cations with Iodide Anions

J. X. Wang,*,† G. M. Watson,‡ and B. M. Ocko‡

Department of Applied Science, Chemical Sciences Division, and Department of Physics, Brookhaven National Laboratory, Upton, New York 11973

Received: October 4, 1995; In Final Form: December 22, 1995[⊗]

Alkali metal cations are found, using X-ray diffraction, to coadsorb with iodide ions on a Au(110) electrode surface at potentials positive of the onset of the Au(110) reconstruction and negative of the formation of iodine monolayers. The adlayer exhibits a $c(2 \times p)$ in-plane diffraction pattern with p depending on the cation species and concentration. For the CsI adlayer, $p = {}^4/_3$ independent of potential and the Cs^+-I^- spacing is close to that in bulk CsI. In KI, NaI, and LiI solutions, p increases with increasing potential. As a result, the coverages of both the cation and anion species decrease with increasing potential. For the anion, the slope of the potential-dependent coverage is opposite of its behavior in the absence of cation coadsorption. This unusual behavior is attributed to the net positive charge within the adlayer due to the partial discharge of chemisorbed iodides. Details of the diffraction features suggest the existence of antiphase domains and relaxation at domain walls.

I. Introduction

The atomic structure and phase behavior of solid−electrolyte interfaces is fundamentally important to our understanding of the microscopic basis of electrochemical phenomena. New *in situ* structural probes, such as, surface X-ray scattering (SXS), scanning tunneling microscopy (STM), and atomic force microscopy, can provide detailed structural information at electrode−electrolyte interfaces on an atomic scale. Most of the adlayer structural studies have been carried out for highly discharged adsorbates, including under potential deposited (UPD) metals[1] and surface oxidized halides.[2−8] These studies have significantly enhanced our understanding of the structure of atomic adlayers and its effect on electrochemical processes. Little is known, however, about the ordering of binary ionic adlayers on single-crystal electrode surfaces.

Ion adsorption on electrodes has been extensively studied theoretically and experimentally as the central component of the electrochemical double-layer models. In a molecular model for anion adsorption at an electrode/electrolyte interface, adsorbed anions are partially solvated, i.e., the dipoles of the solvent molecules at the surface are oriented toward the negative charge of the ad-anions.[9,10] In concentrated electrolytes, the lateral Coulombic repulsion between the ad-anions is likely counterbalanced by cation coadsorption. This possibility has long been recognized but excluded from most molecular models used to describe the properties of the inner layer of the electrical double layer, in part, because of the lack of reliable experimental data.[9]

The cesium ion, as the largest and the least hydrated alkali metal ion, is believed to be the most readily adsorbed cation, and for this reason it has attracted the most attention in experimental studies of cation coadsorption. Surface concentrations of Cs^+, Cl^-, Br^-, and I^- have been determined by *ex situ* X-ray photoelectron spectroscopy as a function of emersion potential from cesium halide on polycrystalline gold films.[11] A significant increase of Cs^+ adsorption in the potential region of the onset of halide adsorption has been demonstrated. A (4 × 4) LEED pattern for a CsI adlayer has been reported for the Au(111) electrode emersed from a CsI solution at potentials negative of −0.4 V,[12] but has not been confirmed by any *in situ* techniques. One possible reason is that the ordering is induced by the crystallization of CsI in the emersion process. Recently, Gao et al. obtained atomically resolved STM images for a cesium−iodide coadsorbed adlayer on Au(110).[4] They suggested a CsI_2 stoichiometry for the adlayer. Here we report *in situ* SXS results for the cation-dependent adlayer structures on Au(110) in CsI, KI, NaI, and LiI solutions. On the basis of the match between the physical properties and observed lattice structures of the adlayers, it is concluded that alkali metal iodides form well-ordered ionic adlayers with a 1:1 stoichiometry on Au(110). The characteristic structure and phase behavior of binary ionic adlayers have been revealed by detailed structural analysis and systematic studies of concentration effects.

II. Experimental Section

In situ SXS measurements were carried out using a Au(110) disk crystal (10 mm diameter by 3 mm) which was oriented within 0.2° from the ⟨110⟩ crystallographic planes. After sputtering and annealing in vacuum, the sample was transferred to an X-ray diffraction cell.[13] Solutions were made from high-purity NaI, KI, CsI, and KF from Aldrich and water purified by means of a Milli-Q system (Millipore Inc.). After being deoxygenated with 99.999% N_2 gas, the solution was injected into the X-ray cell. A thin-layer solution (10−20 μm) was maintained between the electrode surface and the polypropylene X-ray window. All electrode potentials are referenced to a Ag/AgCl(3 M KCl) electrode. X-ray measurements were carried out at room temperature with focused monochromatic radiation ($\lambda = 1.51$ Å) at the National Synchrotron Light Source beamline X22B using a four circle diffractometer. A 3-mrad Soller slit was used in front of the detector to reduce the diffuse scattering background. A rectangular coordinate system was constructed by taking $a = 2.885$ Å and $b = 4.078$ Å within the surface plane, and $c = 2.885$ Å normal to the surface. The scattering vector Q equals (Ha^*, Kb^*, Lc^*) where $a^* = c^* = 2\pi/a =$

† Department of Applied Science.
‡ Department of Physics.
[⊗] Abstract published in *Advance ACS Abstracts,* March 15, 1996.

0022-3654/96/20100-6672$12.00/0

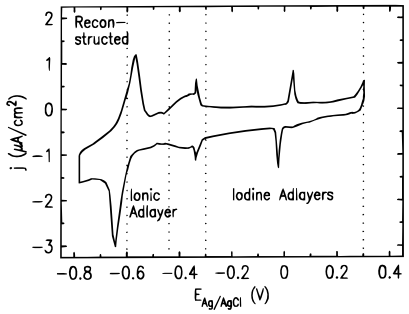

Figure 1. Linear sweep voltammogram for Au(110) in 0.01 M KI. Sweep rate 5 mV/s.

2.178 Å^{-1}, $b^* = 2\pi/b = 1.540$ Å^{-1}. The relationship between the cubic vector, $(h, k, l)_c$, and the rectangular vector (H, K, L) is given by the transformations: $h = -H + L$, $k = H + L$, and $l = K$. For example, $(2, 2, 0)_c = (0, 0, 2)$, $(0, 2, 0)_c = (1, 0, 1)$, and $(1, 1, 1)_c = (0, 1, 1)$. Since all of the in-plane diffraction measurements were carried out at $L = 0.1$, we will abbreviate $(H, K, 0.1)$ as (H, K).

III. Results and Discussion

The electrochemical conditions for the ionic adlayer formation are depicted in Figure 1 by the linear sweep voltammetry curve for Au(100) in 0.01 M KI solution. The pair of peaks near −0.6 V signal the formation (lifting) of the Au(1 × 3) reconstruction[4,14] as the iodide coverage drops below (rises above) a critical value. At −0.34 V the pair of sharp and reversible peaks are associated with the formation and the dissolution of the fully discharged iodine monolayer. Such peaks have also been observed at about the same potential on Au(100) and Au(111) surfaces. Above −0.3 V, several commensurate, uniaxially commensurate, and incommensurate iodine monolayers have been observed in the different potential regions on the three gold surfaces.[6,15] All these iodine adlayer structures have a hexagonal or quasi-hexagonal symmetry and are independent of the cation species as expected for neutral adatoms in an incommensurate or uniaxially commensurate lattice. Furthermore, the electrosorption valence measured at the potentials positive of −0.3 V on Au(111) indicates the complete discharge of iodides.[6] At potentials negative of the formation of iodine monolayer and positive of the reconstruction lifting potential, significant amounts of iodides are adsorbed in a basically ionic form.[16] This can be inferred from the high double-layer capacitance in this potential region.[17] Since the iodide surface oxidation occurs at about the same potential on the three low-index gold surfaces, the potential window of ionic adsorption is the largest for (110) surface because it has the most negative potential of zero charge.

Cyclic voltammograms, obtained respectively in 0.01 M KI and CsI solutions are shown in Figure 2. In order to avoid complications associated with the gold surface reconstruction, the low potential limit is set at −0.6 V compared with the −0.78 V limit in Figure 1. A comparison between the curves in Figure 2 shows a pronounced difference in the potential region between −0.5 and −0.3 V and this is where ionic adsorption occurs. Our X-ray diffraction results (discussed below) show that well-ordered ionic adlayers form between the potential limits marked by the dotted and the dashed vertical lines in Figure 2. In both solutions, at the same negative potential limit, the ordered adlayers disappear and the surface reconstruction of the Au(110) substrate occurs. This phase transition is mainly controlled by the iodide desorption. The positive potential limit, however, differs in these two solutions. In either solution, both correspond to a significant increase of anodic current. These

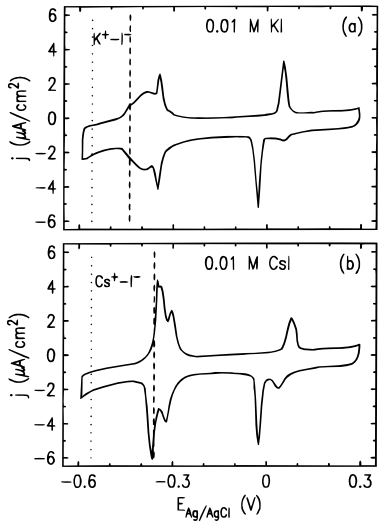

Figure 2. Linear sweep voltammograms for Au(110) in 0.01 M KI (a) and CsI (b) solutions. Sweep rate 20 mV/s.

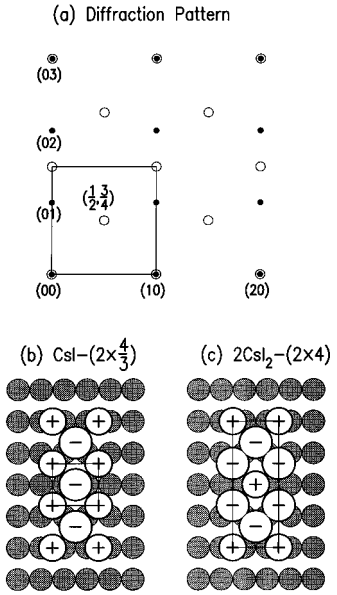

Figure 3. (a) In-plane diffraction pattern observed from the Au(110) electrode at −0.52 V in 0.01 M CsI. Solid and open circles represent the reflections from the Au(110) substrate and the adsorbates, respectively. (b and c) Real space structure models which can give rise to the observed diffraction pattern in a. The diameters of the circles with "−" and "+" signs are respectively proportional to the diameters of the I^- (4.32 Å) and Cs^+ (3.62 Å) relative to the diameter of gold atom (2.885 Å).

facts suggest that the phase transition at higher potentials is associated with not only iodide adsorption but also cation desorption. Between the dashed lines and −0.3 V no ordered adlayer structure is observed. The current peaks in this potential region can be associated with the transitions between the binary ionic adlayer and the fully discharged iodine monolayer.

Figure 3a shows the in-plane diffraction pattern observed for the Au(110) surface at potentials between −0.56 and −0.36 V in 0.01 M CsI solution. In addition to the integer reflections of the Au(110) substrate (solid circles), a centered rectangular diffraction pattern (open circles) is observed and attributed to the Cs^+-I^- adlayer. The base vectors are indexed by ($^1/_2$,0) and (0,$^3/_4$) and all observed diffraction peaks occur at (m/2, 3n/4) where $m + n$ = even. This diffraction pattern corresponds to a centered (2 × $^4/_3$) unit cell in real space. The proposed CsI-(2 × $^4/_3$) adlayer model is shown in Figure 3b. The high-

order commensuration along the ⟨01⟩ direction is illustrated in the figure; however, it does not give rise to the diffraction features of the (2 × 4) surface unit cell since there are no diffraction peaks at the $(0,^1/_4)$ and $(0,^1/_2)$ positions. We did not determine the registry of the adlayer with respect to the underlying gold layers. However, *in situ* STM images have shown that the all the adatoms are located between the rows of Au atoms in the ⟨10⟩ direction and that every "brighter" spot is followed by two "weaker" spots along the ⟨01⟩ direction.[4] This leads to the adlayer registry for a CsI adlayer as shown in Figure 3b in which the "brighter" spots are assigned to the adsorbate, Cs^+ or I^-, on the bridging sites assuming that the tunneling current is mainly determined by the *z* displacement.

Alternatively, the brightness pattern of the STM image can be explained by assuming that the $^1/_3$ of the tunneling maxima appearing "brighter" are associated with Cs^+ and the other $^2/_3$ of the spots appearing "weaker" are associated with I^-. On the basis of this assumption Gao, Edens, and Weaver proposed a CsI_2−(2 × 4) adlayer model[4] as illustrated in Figure 3c. The absence of the diffraction features characteristic of a (2 × 4) surface unit cell precludes significant in-plane relaxations. This means that all the adatoms have to be equally spaced along the ⟨01⟩ direction. In addition, due to the fact that Cs^+ and I^- have an identical number of electrons, the CsI_2 model shown in Figure 3c is practically undistinguishable—from a crystallographic perspective—from the CsI model in Figure 3b. However, as discussed in the following, the former model stands out on the basis of physical and chemical arguments.

The Cs^+−I^- separation calculated from the $(2 \times {}^4/_3)$ unit cell is 3.96 Å, which is very close to the value of 3.95 Å in bulk CsI. This fact shows that the adlayer structure is mainly determined by the adatom−adatom interaction which is consistent with the lack of in-plane relaxation due to the different adsorption sites. In contrast, the I^-−I^- separation of 3.96 Å in the CsI_2 model is much too small compared to the diameter of iodine ions (4.32 Å). Buckling has been ruled out as an explanation since in the model all the iodides are assigned to the "weaker" spots at the near-hollow sites. Besides the strong electrostatic repulsion between the charged iodides, a 3.96 Å nearest-neighbor separation between two iodides is also too small for neutral iodine to be plausible.

The $(2 \times {}^4/_3)$ unit cell of the CsI ionic adlayer has lattice constants 5.77 and 5.55 Å along the ⟨10⟩ and ⟨01⟩ directions, respectively. This is much closer to square than the underlying rectangular gold lattice and is clearly distinct from the quasi-hexagonal symmetry of all three uniaxially incommensurate iodine adlayers found at more positive potentials.[13] For an atomic adlayer, hexagonal symmetry is preferred since it gives the highest number of the nearest neighbors. Square symmetry, on the other hand, is favorable for binary ionic adlayers because it allows each ion to surround itself with the maximum number of counterions. Therefore, the quasi-square symmetry of the lattice supports the binary ionic adlayer model presented in Figure 3b.

Further support for the proposed CsI ionic adlayer structure has been obtained from the congruence of its lattice structure and phase behavior with other alkali-metal iodide adlayers. The diffraction patterns observed in KI, NaI, and LiI solutions have the same symmetry as that of the CsI adlayer. The unit cell in real space is centered rectangular with lattice constants of 2*a* and *pb*, where *p* changes with potential and cation species. Typical *K* scans through the first-order diffraction at $(^1/_2,1/p)$ are shown in Figure 4. The intensity profiles have Lorentzian line shapes as shown by the solid lines. The center of the diffraction peak gives the value of $1/p$. In the CsI solution, the

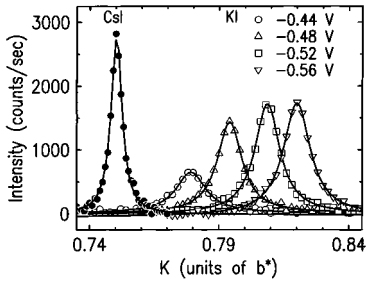

Figure 4. *K* scans at $H = 0.5$ from the $c(2 \times p)$ phase of KI (open symbols) and CsI (solid circles) on Au(110) in 0.01 M solutions. Solid lines are the fits to Lorentzian line shape.

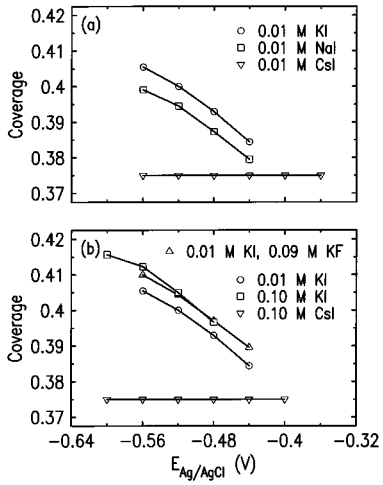

Figure 5. Coverage of iodide as a function of potential in 0.01 M CsI, KI, and NaI solutions (a) and in the solutions containing different K^+ or Cs^+ and I^- concentrations (b).

diffraction intensity profile is centered at 0.75 at all potentials between −0.56 and −0.36 V. Hence, the CsI adlayer is uncompressible with changing potential and has a constant coverage over the 0.2 V potential region. In the KI solution, however, the diffraction peak shifts to larger values in the *K* scans with decreasing potential. Therefore, the lattice constant along the *K* direction decreases and the coverage of the adlayer increases with decreasing potential. The same trend is also observed in NaI and LiI solutions. Since there is one iodide and one cation per unit cell, the iodide coverage is obtained from the ratio of the unit cell areas of the Au(110) surface and the adlayer which is $1/(2p)$. The coverages obtained in various solutions are summarized in Figure 5.

In all the solutions studied, the potential window for the ionic coadsorption shifts negatively with increasing iodide concentration (Figure 5b compared to Figure 5a), independent of the cation species and its concentration. This suggests that the chemisorbed anions play the dominant role in the adsorption process. Within the coadsorption potential window, however, the cation species and concentration are more important in determining the incommensurate adlayer coverage. To demonstrate this effect, we show in Figure 5b that the adlayer coverage at a fixed potential in a mixed solution of 0.1 M K^+ and 0.01 M I^- (triangles) is the same as that in 0.1 M KI solution (squares). Thus, with the exception of Cs^+, higher coverages can be obtained by increasing the cation concentration or decreasing the potential. These effects can be understood in terms of chemisorbed anions and physisorbed cations in the adlayer. The partial discharge of chemisorbed iodides breaks the charge neutrality of the adlayer. The net positive charge within the adlayer increases with increasing the coverage, consistent with higher coverages at more negative potentials.

The K^+-I^- separation in the adlayer ranges from 3.79 Å (at the most negative potential in 0.1 M solution) to 3.92 Å (at the most positive potential in 0.01 M solution). These values are significantly larger than the K^+-I^- separation of 3.525 Å in bulk crystalline KI. Moreover, the NaI coverage as shown in Figure 5a is lower than the KI coverage which means that the cation−iodide separation in the NaI adlayer is larger than that in the KI adlayer despite of the fact that Na^+ are smaller than K^+. The LiI coverage (not shown) is nearly the same as that of KI although the Li^+-I^- separation in the bulk crystal is only 3.002 Å. These facts indicate that the cations, except for Cs^+, appear to be larger in the adlayer than in their corresponding bulk crystals and the difference increases in the order of $K^+ < Na^+ < Li^+$. It is known that the extent of solvation also increases in the same order for these ions,[18] suggesting that the deviation of the cation−iodide separation from the bulk value might be attributed to the partial hydration shell which remains on the cations in the adlayer.[19] This may also be the reason why these three cations all desorb at about the same potential (i.e., the same positive potential for the ionic adlayer, cf. Figure 5), which is significantly more negative than the potential where unhydrated Cs^+ ions desorb. Alternatively, the commensuration along the ⟨10⟩ direction induces a lattice distortion from the square symmetry, which may in turn result in a decrease of packing density of the adlayer as compared to an undistorted square lattice.

We now turn our attention to the detailed structural features of the KI, NaI, and LiI adlayers. The calculated structure factor at (m/2,n/p) for a centered rectangular lattice with one cation (M^+) and one anion (I^-) per unit cell is equal to $(f_{I^-}(-1)^{(m+n)}f_{M^+})$, where we have assumed perfect long-range order of the two components. Thus, the odd-order reflections ($m + n =$ odd) are weaker than the even-order ones. Since iodides and cesium cations have the same number of electrons, i.e., $Z_{I^-} = Z_{Cs^+} = 54$, the structure factor is zero for the odd-order diffractions, which is consistent with the observation of the absence of these reflections. However, $(f_{I^-} - f_{M^+})$ has a nonzero value for other alkali metal cations, and the integrated intensity ratio of odd- and even-order peaks is equal to $((f_{I^-} - f_{M^+})/(f_{I^-} + f_{M^+}))^2$. This yields 0.25, 0.47, and 0.86 for KI, NaI, and LiI adlayers, respectively. In our experiments, a peak with 10% of the peak intensity of the ($^1/_2$,1/p) peak should be visible at ($^1/_2$,0), (0,1/p), and ($^2/_2$,1/p) positions. The absence of these odd-order peaks suggests imperfect long-range order of the binary components in these three adlayers.

The loss of perfect long-range order can be modeled with either "chemical disorder" or antiphase domains. Both give rise to superlattice (odd-order) peaks which are broader than the fundamental (even-order) peaks. By chemical disorder we mean that there is a finite probability that the different chemical species within a unit cell are interchanged, and this gives rise to nearest neighbors of the same species randomly distributed throughout the surface. In the antiphase domain model (described below and shown in Figure 6) the interchanges are confined to the domain walls which run along the commensurate direction. The strain associated with the interchanges is thus limited to the incommensurate direction and can be accommodated by relaxations. Such an anisotropic domain wall model is supported by the observation of anisotropic peak widths at the even-order positions. As we demonstrate below, the relaxation at the domain walls gives rise to peak broadening along the incommensurate direction at the even-order positions which depend on the wave vector. From the analysis of the widths for KI we speculate that the length of the antiphase domains is on average 80 Å. The corresponding superlattice

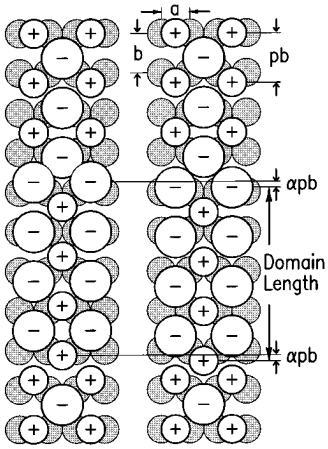

Figure 6. Antiphase domains of a KI adlayer on Au(110) with (right panel) and without (left panel) the lattice displacements, α*pb*, along the ⟨01⟩ direction.

diffraction width, given by the inverse size, is calculated to be 0.0125 $Å^{-1}$ which is about three times wider than the fundamental peak width. Since the superlattice peak intensity relative to the fundamental peak scales as the product of the structure factor ratio squared ($^1/_4$) divided by the width ratio (3), the superlattice peak intensity should be a factor of 12 smaller than the fundamental reflections. Thus, the antiphase domain model for the KI adlayer alone can account for the absence of superlattice peaks under our experimental conditions. To rule out other kinds of disorder, however, requires reliable data for the scattering near the odd-order positions. Detailed analysis of the data in terms of the domain wall relaxation follows.

The left panel of Figure 6 shows an antiphase domain model for the KI adlayer in which the different domains are shifted by exactly a half of a unit cell along both the ⟨10⟩ and ⟨01⟩ directions. That is, the cations and anions are interchanged from one domain to the next. The introduction of these anion- or cation-rich domain walls leads to a lattice relaxation along the incommensurate direction because of the size and charge difference between the different species. This relaxation is represented by a fraction (α) of the adlayer lattice constant (pb) as indicated in the right side of Figure 6. As we shall see, these displacements will give rise to a small shift and a broadening of the diffraction peaks along the displacement direction. It should be made clear that these displacements do not give rise to the incommensurability of the adlayers since the domains themselves are incommensurate with the substrate. A closed-form solution has been obtained by Fenter and Lu for the diffraction intensity profiles from a surface with randomly distributed domain walls.[20] The calculated intensity profile has a Lorentzian line shape along the displacement direction where the full-width half-maximum (FWHM) is given by

$$w = \frac{1}{2\pi}\cos^{-1}\left(2 - \frac{\rho^2 + 1}{2\rho}\right) \qquad (1)$$

where ρ is determined by the domain wall density, γ, and the displacement, α

$$\rho^2 = (1-\gamma)^2 + \gamma^2 + (-1)^{m+1}2\gamma(1-\gamma)\cos(2\pi n\alpha) \qquad (2)$$

Here m and n are the indices of the diffraction peak at (m/2,n/p). A key feature is that the peak width oscillates with increasing n along the displacement direction with a period of 1/α.

In Figure 7, the scattering intensity profiles along the K direction are shown through the three lowest-order diffraction

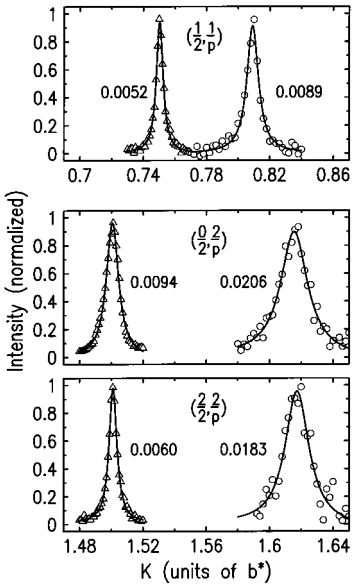

Figure 7. *K* scans through three low-order diffractions of the ionic adlayers at −0.55 V in 0.01 M CsI (trianges) and KI (circles) solutions. After linear background subtraction, peak intensities are normalized to the unity and the solid lines show the fits to Lorentzian line shape. The FWHM of each peak obtained from the fits are given in the units of b^*.

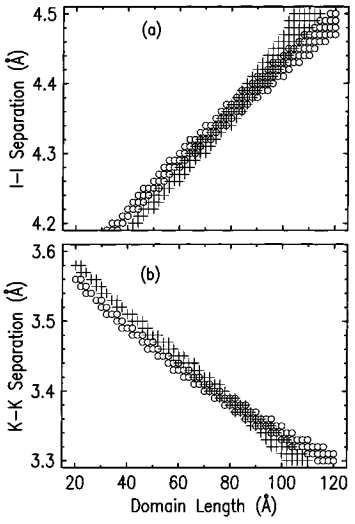

Figure 8. Antiphase domain wall structure parameters (domain length and the nearest-neighbor separations at anion-rich (a) and cation-rich (b) domain walls which yield the measured peak broadening at ($^1/_2$,1/p) (circles) and ($^2/_2$,2/p) (plus signs) positions.

peaks from the CsI (triangles) and the KI (circles) adlayers at −0.55 V. The peak intensities have been normalized to unity to facilitate a comparison of the peak widths. Note that the two *K* scans through $K = 2/p$ have different widths in both solutions as shown in the middle and bottom panels of Figure 7. The *K* scan profiles through the (0,2/p) positions are wider than those through the (2,2/p) positions. This is because the former is along the longitudinal direction where the spectrometer 2θ resolution enters and the latter is partly transverse where the resolution is narrower. To minimize the complications due to the spectrometer resolution in analyzing the *n*-dependent *K* scan widths, only the (2/2,2/p) peak widths will be used, since the (2/2,2/p) position is along the same azimuthal direction as is the (1/2,1/p) position.

The nearly identical peak widths along the *K* direction at ($^1/_2$,1/p) and ($^2/_2$,2/p) for the CsI adlayer indicate that there is no significant lattice displacement in the CsI adlayer. The high-order commensuration probably gives rise to a high energy cost for lattice displacement which inhibits the formation of antiphase domains in the CsI adlayer. In contrast, the ($^2/_2$,2/p) peak is much broader than the ($^1/_2$,1/p) peak for the KI adlayer. This can be due to the lattice displacements at the domain walls as predicted by eqs 1 and 2 or due to the inhomogeneous strain along the incommensurate direction. To distinguish these two peak-broadening mechanisms, data on higher order peaks are required. The former mechanism predicts an oscillation of the peak width with increasing *K*, while the latter suggests a monotonous change. Because of the lack of the data on higher order diffractions (which are too weak to be measured), we have ignored the contribution of the latter mechanism in the following analysis. In doing so, we can, at least, estimate the maximum lattice displacement and domain wall density. With a further assumption that the X-ray coherence length is the same for both the CsI and KI adlayers along the *K* direction (it is true along the *H* direction since the *H* widths are the same for both adlayers), the contribution from the lattice displacement to the peak width is calculated from the difference between the KI and CsI peak widths. The excess widths are 0.0037 and 0.0123 b^* at ($^1/_2$,1/p) and ($^2/_2$,2/p), respectively.

Further analysis of the data proceeds with finding pairs of γ and α which give the measured peak broadening values within ± 0.0002 and ± 0.0006 b^* for the ($^1/_2$,1/p) and ($^2/_2$,2/p) peaks, respectively. The results are plotted in Figure 8 in which the γ and α are respectively converted to the average domain length and the nearest-neighbor separation at the domain walls, D_w. The domain length (cf. Figure 6) is equal to $[(1 - \gamma)/\gamma]pb$.[20] The D_w is calculated from the geometric relation: $D_w^2 = a^2 + ((0.5 \pm \alpha)pb)^2$ where the plus and minus sign give the D_w values corresponding to an expansive and contractive displacements at the anion- and cation-rich domain walls, respectively. In Figure 8, each data point represents a pair of parameters (domain length and D_w) that reproduce the measured peak broadening at ($^1/_2$,1/p) shown as circles and at ($^2/_2$,2/p) shown as plus signs. From the region where the two symbols overlap in the figure, we estimate an average domain length of 80 ± 20 Å, and the D_w of 4.36 ± 0.06 and 3.38 ± 0.06 Å for the anion- and cation-rich domains, respectively. The $I^- - I^-$ and $K^+ - K^+$ separations are both slightly larger than the values, 4.32 and 3.04 Å, respectively, calculated from the ionic radii. This can be attributed to the additional Coulombic repulsion between the neighboring ions with the same charge. From the diffraction data alone, the present model of anion- and cation-rich domain walls is not unique. One alternative model is to replace the extra row of anions or cations by a row of water molecules. This model gives no net charge at the domain wall.

Besides the broadening, a shift of the peak position along the *K* direction is also expected from the displacement at the domain walls and this shift varies with the order of the peak. From the direction of the shifts, one can determine whether expansive (anion rich) or contractive (cation rich or water) displacements are more likely.[20] Calculation with an 80 Å domain length and a 4.36 Å D_w (a set of parameters obtained from analysis of the peak broadening) gives a shift of −0.0039 (δ_1) and −0.0050 (δ_2) b^* at ($^1/_2$,1/p) and ($^2/_2$,2/p), respectively. A positive shift with the same magnitude is obtained when D_w equals to 3.38 Å. The peak positions measured at ($^1/_2$,1/p) and

($^2/_2$,2/p) are 0.809 ± 0.001 and 1.616 ± 0.001, respectively. These give a measured $\delta_1 - \delta_2/2$ value of 0.001 ± 0.002 (0.809 − 1.616/2) which is comparable to the calculated value of ±0.0014 (0.0039 − 0.0050/2). This result demonstrates that the peak widths and the peak shifts are both in agreement with the model. However, it is not possible to speculate on the sign of the displacements at the domain walls since the uncertainty in $\delta_1 - \delta_2/2$ is large. A final note from the analysis is that the coverage is well defined by the position of the ($^1/_2$,1/p) peak because the peak shift due to the domain walls is small relative to the reciprocal lattice constant (0.0039/0.809 = 0.5%).

IV. Conclusions

The results of *in situ* X-ray diffraction experiments demonstrate the coadsorption of four alkali metal cations with specifically adsorbed iodide anions on Au(110). Although SXS does not have element sensitivities, the coadsorption of cations is clearly manifested by the distinct quasi-square symmetry of the $c(2 \times p)$ lattice structure, the unique concentration dependence on both the cation and anion species, and the diffraction pattern and features which are consistent with the antiphase domain wall model. The potential dependence of the adlayer coverage shows that the lateral electrostatic interactions among the ad-ions has pronounced effects not only on the symmetry of the adlayer lattice but also on its cooperative adsorption behavior. These results support the view that cation coadsorption has to be included in the molecular models for a successful description of ion adsorption on metal electrode surfaces in concentrated electrolytes.

Acknowledgment. We thank M. J. Weaver and X. Gao for several enlightening conversations and sending us their manuscripts prior to publication. This work is supported by the Division of Materials Research, U.S. Department of Energy, under Contract No. DE-AC02-76CH00016.

References and Notes

(1) (a) Toney, M. F.; Gordon, J. G.; Samant, M. G.; Borges, G. L.; Melroy, O. R.; Yee, D.; Sorensen, L. B. *J. Phys. Chem.* **1995**, *99*, 4733. (b) Adzic, R. R.; Wang, J.; Vitus, C. M.; Ocko, B. M. *Surf. Sci. Lett.* **1993**, *293*, 876. (c) Wang, J. X.; Adzic, R. R.; Ocko, B. M. *J. Phys. Chem.* **1994**, *98*, 7182. (d) Wang, J. X.; Adzic, R. R.; Magnussen, O. M.; Ocko, B. M. *Surf. Sci.* **1995**, *335*, 120. (e) Wang, J. X.; Adzic, R. R.; Magnussen, O. M.; Ocko, B. M. *Surf. Sci.* **1995**, *344*, 111.

(2) Tao, N. J.; Lindsay, S. M. *J. Phys. Chem.* **1992**, *96*, 5213.

(3) Gao, X.; Weaver, M. J. *J. Am. Chem. Soc.* **1992**, *114*, 8544.

(4) Gao, X.; Edens, G. J.; Weaver, M. J. *J. Phys. Chem.* **1994**, *98*, 8074.

(5) Gao, X.; Edens, G. J.; Liu, F.-C.; Hamelin, A.; Weaver, M. J. *J. Phys. Chem.* **1994**, *98*, 8086.

(6) Ocko, B. M.; Watson, G. M.; Wang, J. *J. Phys. Chem.* **1994**, *98*, 897.

(7) (a) Magnussen, O. M.; Ocko, B. M.; Adzic, R. R.; Wang, J. X. *Phys. Rev. B* **1995**, *51*, 5510. (b) Magnussen, O. M.; Ocko, B. M.; Wang, J. X.; Adzic, R. R. *J. Phys. Chem.* **1996**, *100*, 5500.

(8) Wandlowski, Th.; Wang, J. X.; Magnussen, O. M.; Ocko, B. M. *J. Phys. Chem.*, submitted for publication. Ocko, B. M.; Magnussen, O. M.; Wang, J. X.; Wandlowski, Th. *Phys. Rev. B*, **1996**, *53*, 7654.

(9) Lamperski, S. *J. Electroanal. Chem.* **1994**, *379*, 445.

(10) Stern, O. *Z. Elektrochem.* **1924**, *30*, 508.

(11) Kolb, D. M.; Rath, D. L.; Wille, R.; Hansen, W. N. *Ber. Bunsen-Ges. Phys. Chem.* **1983**, *87*, 1108.

(12) Bravo, B. G.; Michelhaugh, S. L.; Soriaga, M. P.; Villegas, I.; Suggs, D. W.; Stickney, J. L. *J. Phys. Chem.* **1991**, *95*, 5245.

(13) Wang, J. X.; Davenport, A. J.; Isaacs, H. S.; Ocko, B. M. *Phys. Rev. B* **1992**, *46*, 10321.

(14) Ocko, B. M.; Helegesen, G.; Schardt, B.; Wang, J.; Hamelin, A. *Phys. Rev. Lett.* **1992**, *69*, 3350.

(15) (a) Wang, J. X.; Watson, G. M.; Ocko, B. M. Manuscript in preparation. (b) Ocko, B. M.; Magnussen, O. M.; Wandlowski, Th.; Wang, J. X. Manuscript in preparation.

(16) The word "ionic" used here does not bear any quantitative meaning on how much charge remains on the chemisorbed iodides, but is used to make a clear distinction from the fully discharged iodines at more positive potentials.

(17) Hamelin, A.; Bellier, P.-P. *Surf. Sci.* **1978**, *78*, 159.

(18) Burgess, J. In *Metal Ions in Solution*; John Wiley & Sons: New York, 1984.

(19) The partial hydration and the effective size of ad-ions have also been used for anions, for example, in: Lamperski, S. *J. Electroanal. Chem.* **1994**, *379*, 445.

(20) (a) Fenter, P.; Lu, T.-M. *Surf. Sci.* **1985**, *154*, 15. (b) Lu, T.-M.; Lagally, M. G. *Surf. Sci.* **1982**, *120*, 47.

JP952938Y